Received: 30 June 2018 | Revised: 19 November 2018 | Accepted: 19 November 2018

DOI: 10.1002/jrs.5539

RESEARCH ARTICLE

WILEY Journal of RAMAN SPECTROSCOPY

Symmetries of modes in $Ni_3V_2O_8$: Polarized Raman spectroscopy and ab initio phonon calculations

Swayam Kesari[1,2] | Rekha Rao[1,2] | Mayanak K. Gupta[1] | R. Mittal[1,2] | Geetha Balakrishnan[3]

[1]Solid State Physics Division, Bhabha Atomic Research Centre, Mumbai, India

[2]Homi Bhabha National Institute, Mumbai, India

[3]Department of Physics, University of Warwick, Coventry, UK

Correspondence
Rekha Rao, Solid State Physics Division, Bhabha Atomic Research Centre, Mumbai 400085, India.
Email: rekhar@barc.gov.in

Funding information
EPSRC, UK, Grant/Award Number: EP/M028771/1

Abstract

Knowledge of symmetries of vibrational modes is essential for understanding the mechanism of structural transitions and spin-phonon coupling in multiferroics where phonons play a vital role. Using polarized Raman spectroscopy, we have identified and assigned symmetries of 30 out of the 36 expected Raman active modes in $Ni_3V_2O_8$. The zone-centred phonon mode wavenumbers are calculated using ab initio calculations. The gerade mode wavenumbers are compared with our polarized Raman data whereas ungerade mode wavenumbers are compared with the reported infrared measurements and a good agreement was observed between the experimentally measured wavenumbers and the calculated wavenumbers. The displacements of different types of vibrations calculated and visualized using ab initio phonon calculation are presented. These assignments will be useful for visualization of Raman modes that may be sensitive to different magnetic states and to explore spin–lattice coupling across magnetic transitions.

KEYWORDS

ab initio calculations, displacements of phonon modes, gerade and ungerade modes, polarized Raman spectroscopy, symmetries of Raman active modes

1 | INTRODUCTION

Magnetic frustration systems are multiferroic materials in which magnetism and ferroelectricity may coexist and interact with each other. In the search of multiferroic materials, the magnetic-frustrated system $Ni_3V_2O_8$ (NVO) is one of the most investigated material.[1–8] The compound NVO is paramagnetic at ambient conditions and shows several magnetic phase transitions at low temperatures. Below 9.8 K, incommensurate (IC) sinusoidal spin structure appears that changes to helical spin structure below 6.5 K, and a commensurate magnetic structure appears below 3.9 K.[1,2,7] The magnetic ordering drives the ferroelectric order that appears in the temperature range of 3.9–6.5 K with a spontaneous polarization along the *b*-axis and forms a type II multiferroic material and has been the matter of investigation recently.[2–4] It is speculated that small lattice displacements due to controlled introduction of lattice strain can tune the ferroelectricity, and it is reported that ferroelectricity can be completely suppressed to 6.2 K by applying pressure.[5]

Many of the magnetic transitions, especially in type II multiferroics, involve coupling of spin with phonons, which can be probed spectroscopically. A detailed Raman spectroscopic study can reveal the interplay of structure and magnetic and ferroelectric properties. Hence, several magnetic- and spin-frustrated systems are extensively explored using Raman spectroscopy across the transition temperature with an interest of phonon-spin anomalies. Local changes in bond length and bond angles across magnetic/ferroelectric transitions manifest themselves as changes in phonon wavenumbers. Information about

the symmetry of the modes is essential for understanding any phonon-assisted phenomena such as structural transitions involving phonon softening or spin-phonon coupling. Even origin of stimulated Raman scattering in PbB_4O_7 is identified by a polarization-dependent studies on single crystals.[9] In the series $RCrO_3$ (R = La, Pr, Nd, and Sm),[10] evolution of phonon wavenumber as a function of orthorhombic distortion and mode-mixing behaviour was understood using assignment of vibrational modes by polarized Raman study. A detailed Raman and FTIR investigations on $Na_2Ti_3O_7$ enabled assignments of all the vibrational modes, which is useful for technological applications of the compound.[11] Polarized Raman investigation has explained the temperature-dependent phase transitions in single crystals of Sc_3CrO_6,[12] and assignment of not only phonons but also magnons was done in CuB_2O_4 using polarized Raman spectroscopy.[13] It has been used to understand the mechanism of ferroelectric to paraelectric transition in bulk $BaTi_2O_5$[14] as well as in thin films.[15] Many magnetic systems have been explored using Raman spectroscopy across magnetic transitions with the interest of phonon-spin anomalies. Although $CaFe_2O_4$ has shown no phonon anomaly near transition temperature,[16] the anomalies close to the transition temperature are discussed in $PrMnO_3$, $NdMnO_3$, $TbMnO_3$, and $DyMnO_3$ using polarized Raman spectroscopy[17] and the phonon anomalies observed in $BaFe_2As_2$,[18] which are attributed to spin–lattice electronic coupling. Polarized Raman measurements enabled observation of transient lattice disorder in very narrow temperature intervals at the onset of the multiferroic ordering in $Eu_{(1-x)}Ho_xMnO_3$[19] and Higgs modes in the 2-D antiferromagnet Ca_2RuO_4 providing strong evidence for excitonic magnetism in it.[20] Recently, polarization-dependent micro-Raman studies are shown to be useful for assignment of Raman modes even in polycrystalline ceramics.[21]

In NVO, information of vibrational symmetry modes is available only for the infrared (IR) modes.[6] A detailed inelastic neutron-scattering measurement has reported phonon density of states, and polarized IR spectroscopic study has given the symmetries of IR modes along with first principles calculations of IR wavenumbers.[6] Temperature-dependent infrared spectroscopic studies have indicated that the lattice is flexible and sensitive to magnetic transitions.[8] Though there exists report on Raman study on NVO and its solid solutions with substituted Co, Cu, and so forth,[22–24] the symmetries of Raman active modes are not reported. The symmetries of Raman active modes of a similar compound $SrNi_2V_2O_8$ have been identified by using polarized Raman spectroscopy,[25] but it crystallizes into a tetragonal phase where as NVO is orthorhombic[26] at ambient conditions. The observation of lesser number of modes in $SrNi_2V_2O_8$ than group theoretically predicted number is modelled on the basis of the local symmetry considerations.

Here, we report polarized Raman spectroscopic measurements carried out on single crystal of $Ni_3V_2O_8$ to identify the symmetry of Raman active modes and ab initio DFT calculations. The IR mode wavenumbers and their symmetries are also computed using ab initio calculations, which are then compared with the existing report.[6]

2 | EXPERIMENTAL DETAILS

Polycrystalline NVO is synthesized by solid-state reaction by using stoichiometric amounts of NiO and V_2O_5. Raman spectroscopic measurements have been carried out by using ~15 mW, 532 nm laser. The backscattered light is analysed using in-house 0.9-m single monochromator[27] coupled with an edge filter and detected by a cooled CCD with sample in vertical geometry.

Single crystal of NVO was grown by floating zone technique in a four-mirror image furnace, which is described in detail in Balakrishnan et al[28] and aligned by X-ray Laue method. For polarized Raman spectroscopic measurements, we have mounted the oriented single crystal of size $2 \times 2 \times 1$ mm^3 on a goniometer for finer alignment. The back-scattered light from single crystal in different geometries is selected through analyser. Raman spectra at 77 K were recorded using a Linkam temperature Stage (THMS-600) for polycrystalline as well as for single crystal. Polarized Raman spectra were recorded in six orientations at room temperature and in selected geometry at 77 K.

3 | CALCULATION DETAILS

The lattice dynamics calculations have been performed using ab initio method. Density functional theory (DFT) has been shown to describe the structural and lattice dynamical properties of material using pseudo potentials and plane wave basis sets. The phonon wavenumbers have been calculated in the framework of density functional perturbation theory (DFPT).[29] The relaxed geometries and total energies were obtained using the projector-augmented wave (PAW) formalism[30,31] of the Kohn–Sham density functional theory,[32,33] within the generalized gradient approximation (GGA), implemented in the Vienna ab initio simulation package (VASP).[34] The GGA was formulated by the Perdew–Burke–Ernzerhof (PBE) density functional.[35] The valence electronic configurations of Ni, V, and O as used in calculations for pseudo potential generation are $p^6d^8s^2$, $s^2p^6d^3s^2$, and s^2p^4, respectively. We have performed spin-

polarized calculations in antiferromagnetic structure. The on-site Hubbard correction is applied on d- orbital of Ni and V using the Dudarev approach[36] using U_{eff} = 3.25 and 6.24 eV, respectively. These U_{eff} values are obtained from reference,[37] which reproduces the closest experimental structure as well as the zone centre phonon wavenumbers.

All results were well converged with respect to *k*-mesh and energy cut-off for the plane wave expansion. The break conditions for the self-consistent field (SCF) and for the ionic relaxation loops were set to 10^{-8} eV and 10^{-5} eV Å^{-1} respectively. The latter break condition means that the obtained Hellmann–Feynman forces are less than 10^{-5} eV Å^{-1}. A 4 × 4 × 4 *k*-point mesh for the Brillouin zone integration was found to be suitable for the required convergence. The energy cut-off was set to 800 eV.

4 | RESULTS AND DISCUSSION

4.1 | Irreducible representation and polarization-selection rule for polarized Raman spectroscopy in NVO

The crystal structure of NVO at ambient conditions is orthorhombic with space group *Cmca* (No. 64), Z = 2.[26] It consists of edge-sharing NiO_6 octahedra and VO_4 tetrahedra with one type of VO_4 tetrahedra and two types of NiO_6 octahedra. As there are two formula units per unit cell at ambient conditions, there are 78 normal modes in NVO. The symmetries and wavenumbers of these normal modes can be obtained by diagonalizing the dynamical matrix using the site symmetry information of each atom in the unit cell. These individual diagonalized modes are called as irreducible representations. Though group theoretical transformations in irreducible representations of symmetry modes in NVO are reported,[3,6,22] we have determined these transformations using nuclear site group analysis described in Rousseau et al.[38]

From reported X-ray diffraction data, the structure of NVO consists of Ni1 atom occupying 4*a* Wyckoff position, the 8*e* Wyckoff position is occupied by Ni2 atom, 8*f* Wyckoff position is occupied randomly by V1, O1 and O2 atoms, and 16*g* Wyckoff position is occupied by O3 atom.[3,6,22] Following the nuclear site group analysis described in Rousseau et al[38] for space group *Cmca*, it gives the point group symmetry for all these Wyckoff positions and the transformation in the corresponding irreducible representations. The transformations obtained in irreducible representations along with the Wyckoff position of different atoms are tabulated in Table S1. This table shows that the dynamical matrix transforms in to 78 non-degenerate irreducible representations. The total transformations are as follows

$$\Gamma = 10A_g + 8B_{1g} + 7B_{2g} + 11B_{3g} + 8A_u + 13B_{1u} + 12B_{2u} + 9B_{3u}.$$

As NVO is a centro-symmetric compound, its IR and Raman active modes will be mutually exclusive. The three ungerade B_{1u}, B_{2u}, and B_{3u} symmetry modes are acoustic, the 31 ungerade B_{1u}, B_{2u}, and B_{3u} symmetry modes are IR active, and the remaining eight ungerade A_u symmetry

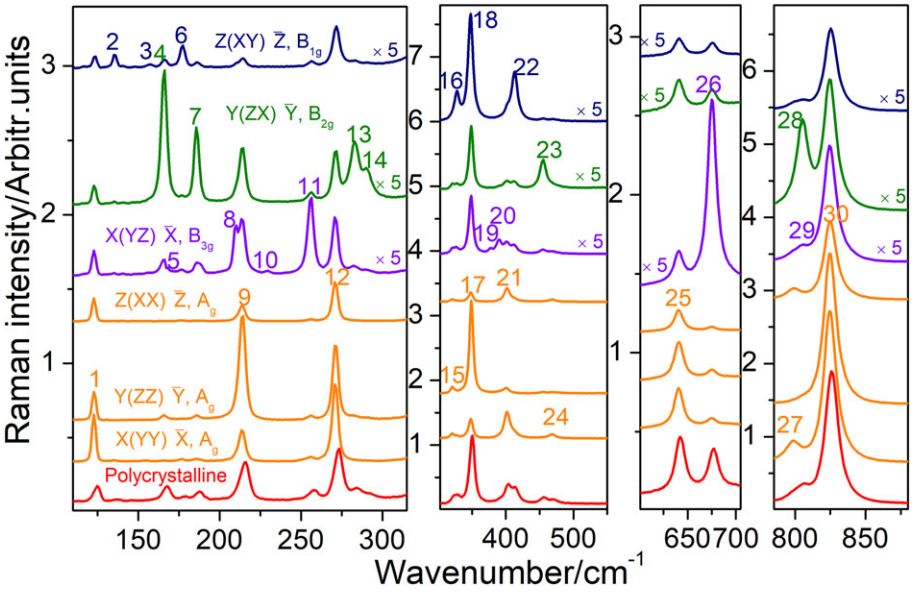

FIGURE 1 Raman spectra of polycrystalline NVO and single crystal NVO in different orientations at ambient conditions [Colour figure can be viewed at wileyonlinelibrary.com]

TABLE 1 Raman mode wavenumbers and their symmetries at ambient conditions obtained from polarized Raman spectroscopy and comparison of it with gerade modes calculated by ab initio calculations at zone centre

Symmetry	Mode index	Wavenumber (cm^{-1})	
		Polarized Raman experiment	Calculated (gerade modes at zone centre)
A_g	1	123	125
A_g	9	213	248
A_g	12	271	274
A_g	15	320	342
A_g	17	348	382
A_g	21	401	440
A_g	24	469	492
A_g	25	641	658
A_g	27	799	802
A_g	30	825	839
B_{1g}	2	135	128
B_{1g}	3	157	157
B_{1g}	6	177	211
B_{1g}	16	328	323
B_{1g}	18	351	359
B_{1g}		N.O.	384
B_{1g}	22	413	434
B_{1g}		N.O.	784
B_{3g}	5	168	176
B_{3g}	8	210	201
B_{3g}	10	256	260
B_{3g}	11	230	268
B_{3g}		N.O.	339
B_{3g}	19	378	412
B_{3g}	20	390	422
B_{3g}		N.O.	483
B_{3g}	26	675	685
B_{3g}		N.O.	824
B_{3g}	29	806	845
B_{2g}	4	166	163
B_{2g}	7	186	226
B_{2g}	13	283	321
B_{2g}	14	291	339
B_{2g}	23	455	469
B_{2g}		N.O.	480
B_{2g}	28	805	796

Note. Peaks are indexed with integers in the spectra in increasing order of wavenumber. N.O.: modes that are not observed.

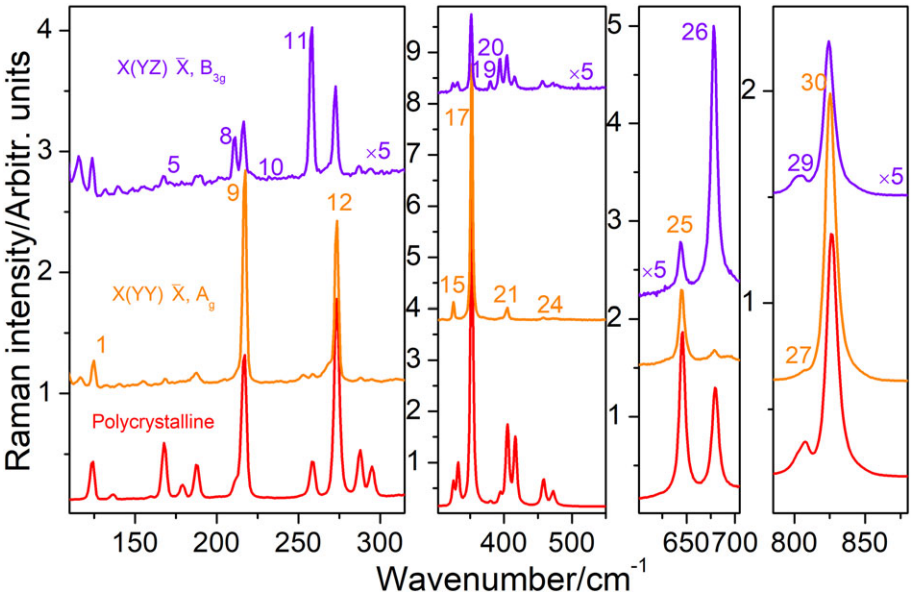

FIGURE 2 Raman spectra of polycrystalline NVO and single crystal NVO in $X\,(YY)\overline{X}$ and $X\,(YZ)\overline{X}$ geometries at 77 K [Colour figure can be viewed at wileyonlinelibrary.com]

modes are optically inactive. The 36 gerade A_g, B_{1g}, B_{2g}, and B_{3g} symmetry modes are all Raman active.

Raman modes of a solid and the Raman tensor associated with it are dependent on the symmetry of the crystal. The form of the Raman tensor will give the direction of polarization of scattered light, and non-vanishing entry in its matrix is a pre-requisite to observe a Raman mode. However, intensity of the Raman mode will also depend on various other factors such as wavelength of the excitation source and detector response at that wavelength.

The 36 Raman active modes in NVO that transform with following symmetries

$$\Gamma^{\text{Raman}} = 10A_g + 8B_{1g} + 7B_{2g} + 11B_{3g}.$$

The matrix notations of Raman tensors of these symmetries are taken from Loudon,[39] which are as follows

$$A_g = \begin{bmatrix} a & 0 & 0 \\ 0 & b & 0 \\ 0 & 0 & c \end{bmatrix} \quad B_{1g} = \begin{bmatrix} 0 & d & 0 \\ d & 0 & 0 \\ 0 & 0 & 0 \end{bmatrix}$$

$$B_{2g} = \begin{bmatrix} 0 & 0 & e \\ 0 & 0 & 0 \\ e & 0 & 0 \end{bmatrix} \quad B_{3g} = \begin{bmatrix} 0 & 0 & 0 \\ 0 & 0 & f \\ 0 & f & 0 \end{bmatrix}.$$

As the present crystal system is an orthogonal system and these matrices are mutually orthogonal, it is possible to orient the single crystal such that both the laboratory frame and crystal frame can have common axes. From the non-zero entries in these matrices, it is clear that the Raman spectra recorded in the geometries $X\,(YY)\overline{X}$, $X\,(ZZ)\overline{X}$, $Y\,(XX)\overline{Y}$, $Y\,(ZZ)\overline{Y}$, $Z\,(XX)\overline{Z}$, and $Z\,(YY)\overline{Z}$ will have modes of only A_g symmetry. To get the modes of symmetries B_{1g}, B_{2g}, and B_{3g}, we need to record the Raman spectra in $Z\,(XY)\overline{Z}$, $Y\,(ZX)\overline{Y}$, and $X\,(YZ)\overline{X}$ geometries, respectively.

4.2 | Polarized Raman spectroscopy and symmetry of Raman active modes in NVO

Raman spectra of single crystal NVO in different geometries are shown in Figure 1 along with the Raman spectra of polycrystalline NVO at ambient conditions. The spectra match well with the reported.[22–24] In our present study with better resolved spectra, we have identified the symmetries of 30 observed modes using polarized Raman spectroscopy. The modes between 500 and 900 $cm^{-1}$are predominantly due to V-O stretching but because O-atoms are also connected to Ni atoms, these modes are mixed with some Ni-O stretching/bending. The modes between 200 and 500 cm^{-1} are O-V-O and O-Ni-O bending modes. The modes below 200 cm^{-1} are rigid motions of NiO_6 octahedra and VO_4 tetrahedra.

For identifying the symmetric modes (A_g), we have recorded the Raman spectra in three geometries $X\,(YY)\overline{X}$, $Y\,(ZZ)\overline{Y}$, and $Z\,(XX)\overline{Z}$, and the normalized spectra are shown in Figure 1. Raman spectra in these three geometries clearly provided us all the expected modes of A_g symmetry, which are indexed as shown. Some very weak peaks appearing in these three spectra are due to leakage of strong antisymmetric modes, which could be due to slight mis-orientation.

For identifying the B_{1g}, B_{2g}, and B_{3g} symmetry modes, we have recorded the Raman spectra in $Z\,(XY)\overline{Z}$, $Y\,(ZX)\overline{Y}$, and $X\,(YZ)\,\overline{X}$ geometries, respectively, which are also represented in Figure 1. It is clear from Figure 1 that we have identified six out of eight expected modes of B_{1g} symmetry, six out of seven expected modes of B_{2g} symmetry, and eight out of 11 expected modes of B_{3g} symmetry. The modes are indexed with the integers as shown in Figure 1. In all these spectra, the appearance of symmetric mode can also be seen but are weak. The mode wavenumbers along with the symmetries of these modes are listed in the Table 1.

Figure 2 represents Raman spectra of single crystal NVO in $X\,(YY)\overline{X}$ and $X\,(YZ)\overline{X}$ geometries along with polycrystalline NVO at 77 K. There is not much difference between the Raman spectra at 77 K and at ambient conditions except for the mode separation, which is consistent with the report that there is no structural change in NVO up to 77 K. The Raman spectra recorded in $X\,(YY)\overline{X}$ and $X\,(YZ)\overline{X}$ geometries at 77 K have given the same number of modes of symmetries A_g and B_{3g}, respectively, as obtained at ambient conditions. In this case, the peaks are better resolved, which clearly confirms the existence of nearly overlapping modes at ambient conditions. The modes are indexed similar to that at ambient conditions.

Finally, we have identified 30 out of 36 expected Raman active modes and assigned their symmetries. The reason of not observing the remaining modes ($2B_{1g}$, $1B_{2g}$, and $3B_{3g}$) could be due to of their weak intensity or their overlapping with other modes due to accidental degeneracy.

4.3 | Ab initio calculations of zone centre phonons in NVO

The compound NVO is known to exhibit a rich magnetic phase diagram with temperature. It shows high- and low-temperature incommensurate (IC) phases (HTI and LTI) and two commensurate (C and C′) spin structures.[1,7] The magnetic structure in these phases is noncollinear. Yildirim et al[6] have performed the calculation in collinear magnetic structure, but we have found that in antiferromagnetic configuration, collinear calculation breaks the symmetry of the structure. In order to preserve the symmetry, we have performed magnetic structure calculation in noncollinear spin configuration. There are only a few antiferromagnetic configurations other than ferromagnetic configuration allowed to retain the orthorhombic structure of NVO. In Figure S1, we have described the antiferromagnetic structure used in the calculation where the spin direction of Ni1 is along *a*-axis, whereas Ni2 spin lies along *b*-direction to retain the orthorhombic symmetry. We have relaxed the structure in this antiferromagnetic configuration, and the relaxed structural parameters are given in Table S2. We have found a good agreement with the reported measurements.[26] Some of the zone centre phonon wavenumbers show marginal change in wavenumber in different magnetic states.

TABLE 2 The calculated wavenumber of ungerade modes and their comparison with reported[6] infrared data and ab initio calculations

	Reported[6]		Calculated (ungerade modes at zone centre)
	Experiment (IR)	Ab initio calculation	
B_{1u}	N.O.	143	129
B_{1u}	188	185	186
B_{1u}	219	213	212
B_{1u}	257	253	259
B_{1u}	303	302	296
B_{1u}	323	314	346
B_{1u}	N.O.	331	355
B_{1u}	373	376	396
B_{1u}	N.O.	455	485
B_{1u}	629	665	650
B_{1u}	787	816	794
B_{1u}	825	833	827
B_{2u}	174	172	155
B_{2u}	201	196	198
B_{2u}	224	221	249
B_{2u}	290	291	285
B_{2u}	329	320	350
B_{2u}	323	327	355
B_{2u}	407	405	437
B_{2u}	453	449	476
B_{2u}	631	676	654
B_{2u}	810	829	819
B_{2u}	881	892	851
B_{3u}	N.O.	148	132
B_{3u}	203	197	189
B_{3u}	240	243	244
B_{3u}	309	313	346
B_{3u}	335	337	371
B_{3u}	370	376	403
B_{3u}	424	425	439
B_{3u}	787	808	795

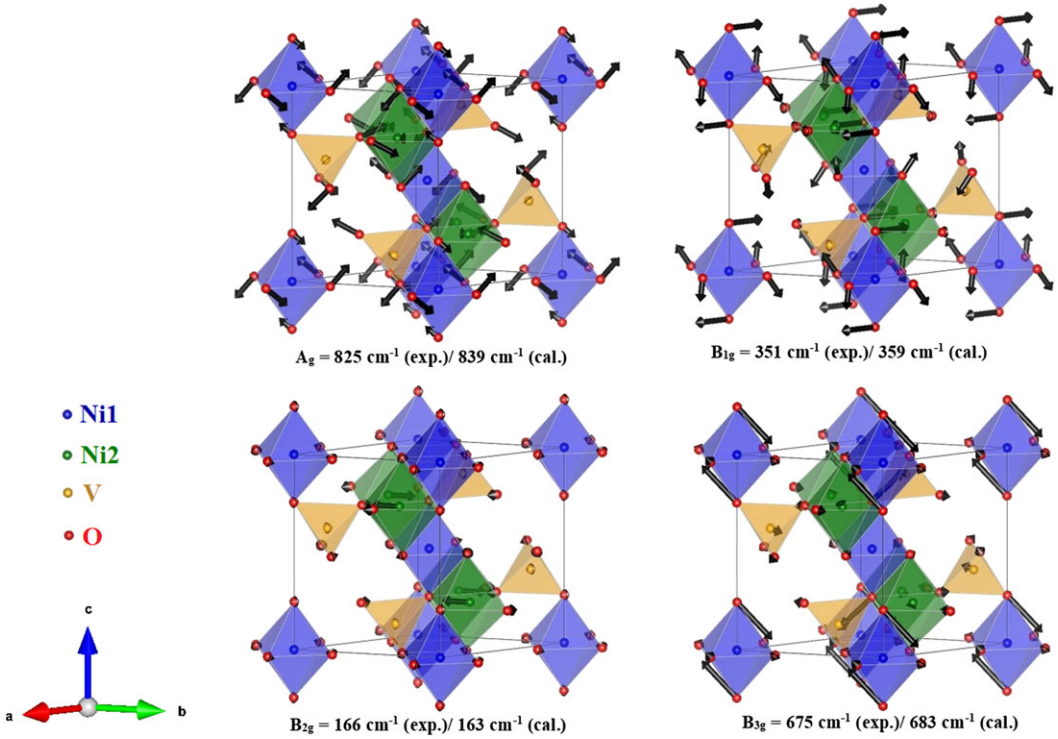

FIGURE 3 Computed atomic displacement for some of the prominent modes of NVO. The structure consists of three types of polyhedral units. VO_4 tetrahedral units are shown by yellow colour, and two different nickel octahedral units $Ni1O_6$ and $Ni2O_6$ are shown by blue and green colour, respectively. V: yellow; Ni1: blue; Ni2: green; O: red [Colour figure can be viewed at wileyonlinelibrary.com]

The mode wavenumbers with gerade symmetry are tabulated in Table 1 and compared with the present polarized Raman measurements. The ungerade symmetry modes other than optically inactive A_u modes are tabulated in Table 2, which is compared with the previous available measurements and calculations.[6] We have found a fair agreement between calculation and present measurements. The calculated optically inactive modes of symmetry A_u are tabulated in Table S3. In Figure 3, we have shown the displacement pattern of a few phonon modes prominently observed in Raman measurements. The displacement pattern of the highest energy A_g mode at 839 cm^{-1} shows the stretching of V-O bonds in VO_4 polyhedral units. As structure of $Ni_3V_2O_8$ consists of corner-shared polyhedral units of $Ni1O_6$ (blue octahedral units in Figure 3), $Ni2O_6$ (green octahedral units in Figure 3), and of VO_4 (yellow tetrahedral units in Figure 3), the dynamics of V-O stretching will also rotate the nickel octahedral units. Another high energy mode that is prominent in Raman measurements is at 685 cm^{-1} of B_{3g} character. This mode involves the displacement of one tetrahedral oxygen, whereas other oxygens are almost at rest. This kind of dynamics will form asymmetric stretching of VO_4 polyhedral units. This will also cause distortion and rotation of nickel octahedral units. The B_{1g} mode at 359 cm^{-1} will involve bending of O-Ni-O bonds as well as rotation of $Ni1O_6$ units and stretching of Ni-O bonds in $Ni2O_6$ units. However, the VO_4 units show distortion due to V-O stretching and O-V-O bending. Interestingly, the B_{2g} mode at 163 cm^{-1} involves only Ni dynamics in $Ni2O_6$ unit, whereas other atom displacements are insignificant. The displacement of Ni will form asymmetric stretching of O-Ni-O linkage. The displacements of all the 75 optical modes are shown in the Supporting Information as in Figure S3. This visualization of Raman modes will be useful in interpreting changes taking place across magnetic transitions and to investigate spin–lattice coupling.

5 | CONCLUSION

With polarized Raman spectroscopic studies, we have assigned 30 out of 36 Raman active modes in NVO. These measurements are further supported by ab initio calculations of zone-centred phonon wavenumbers. Calculated wavenumbers are in fair agreement with Raman and IR measurements. We have identified symmetries of various Raman and IR active modes and provided the displacement pattern of these vibrational modes. The information of symmetries of these Raman and IR active modes will be useful for predicting phonon behaviour and hence the properties of the compound under different thermodynamic conditions.

ACKNOWLEDGEMENT

The work at the University of Warwick was supported by a grant from the EPSRC, UK (EP/M028771/1).

ORCID

Rekha Rao https://orcid.org/0000-0002-1848-6171

REFERENCES

[1] G. Lawes, M. Kenzelmann, N. Rogado, K. H. Kim, G. A. Jorge, R. J. Cava, A. Aharony, O. Entin-Wohlman, A. B. Harris, T. Yildirim, Q. Z. Huang, *Phys. Rev. Lett.* **2014**, *93*(24), 247201.

[2] G. Lawes, A. B. Harris, T. Kimura, N. Rogado, R. J. Cava, A. Aharony, O. Entin-Wohlman, T. Yildirim, M. Kenzelmann, C. Broholm, A. P. Ramirez, *Phys. Rev. Lett.* **2005**, *95*(8), 087205.

[3] A. B. Harris, T. Yildirim, A. Aharony, O. Entin-Wohlman, *Phys. Rev. B* **2006**, *73*(18), 184433.

[4] R. C. Rai, J. Cao, S. Brown, J. L. Musfeldt, D. Kasinathan, D. J. Singh, G. Lawes, N. Rogado, R. J. Cava, X. Wei, *Phys. Rev. B* **2006**, *74*(23), 235101.

[5] R. P. Chaudhury, F. Yen, C. R. D. Cruz, B. Lorenz, Y. Q. Wang, Y. Y. Sun, C. W. Chu, *Phys. Rev. B* **2007**, *75*(1), 012407.

[6] T. Yildirim, L. I. Vergara, J. Íñiguez, J. L. Musfeldt, A. B. Harris, N. Rogado, R. J. Cava, F. Yen, R. P. Chaudhury, B. Lorenz, *J. Phys. Condens. Matter* **2008**, *20*(43), 434214.

[7] N. R. Wilson, O. A. Petrenko, G. Balakrishnan, *J. Phys. Condens. Matter* **2007**, *19*(14), 145257.

[8] L. I. Vergara, J. Cao, N. Rogado, Y. Q. Wang, R. P. Chaudhury, R. J. Cava, B. Lorenz, J. L. Musfeldt, *Phys. Rev. B* **2009**, *80*, 052303.

[9] J. Hanuza, M. Maczka, J. Lorenc, A. A. Kaminskii, P. Becker, L. Bohatý, *J. Raman Spectrosc.* **2008**, *39*, 409.

[10] N. R. Camara, V. T. Phuoc, I. Monot-Laffez, M. Zaghrioui, *J. Raman Spectrosc.* **2017**, *48*, 1839.

[11] F. L. R. E. Silva, A. A. A. Filho, M. B. da Silva, K. Balzuweit, J. L. Bantignies, E. W. S. Caetano, R. L. Moreira, V. N. Freire, A. Righi, *J. Raman Spectrosc.* **2018**, *49*, 538.

[12] N. D. Todorov, M. V. Abrashev, S. C. Russev, V. Marinova, R. P. Nikolova, B. L. Shivachev, *Phys. Rev. B* **2012**, *85*(21), 214301.

[13] V. G. Ivanov, M. V. Abrashev, N. D. Todorov, V. Tomov, R. P. Nikolova, A. P. Litvinchuk, M. N. Iliev, *Phys. Rev. B* **2013**, *88*, 094301.

[14] S. Tsukada, Y. Fujii, Y. Yoneda, H. Moriwake, A. Konishi, Y. Akishige, *Phys. Rev. B* **2018**, *97*(2), 024116.

[15] Y. I. Yuzyuk, J. L. Sauvajol, P. Simon, V. L. Lorman, V. A. Alyoshin, I. N. Zakharchenko, E. V. Sviridov, *J. Appl. Phys.* **2003**, *93*(12), 9930.

[16] N. Kolev, M. N. Iliev, V. N. Popov, M. Gospodinov, *Solid State Commun.* **2003**, *128*(4), 153.

[17] S. Mansouri, S. Jandl, A. Mukhin, V. Y. Ivanov, A. Balbashov, *Sci. Rep.* **2017**, *7*(1), 13796.

[18] A. Baum, Y. Li, M. Tomić, N. Lazarević, D. Jost, F. Löffler, B. Muschler, T. Böhm, J. H. Chu, I. R. Fisher, R. Valentí, *Phys. Rev. B* **2018**, *98*, 075113.

[19] S. Elsässer, A. A. Mukhin, A. M. Balbashov, J. Geurts, *Phys. Rev. B* **2018**, *97*, 224307.

[20] S. M. Souliou, J. Chaloupka, G. Khaliullin, G. Ryu, A. Jain, B. J. Kim, M. Le Tacon, B. Keimer, *Phys. Rev. Lett.* **2017**, *119*(6), 067201.

[21] A. Dias, R. L. Moreira, *J. Raman Spectrosc.* **2018**, *49*, 1514.

[22] Y. S. Seo, S. H. Kim, J. S. Ahn, I. K. Jeong, *J. Korean Phys. Soc.* **2013**, *62*(1), 116.

[23] A. Kumarasiri, G. Lawes, *Phys. Rev. B* **2011**, *84*(6), 064447.

[24] C. Sudakar, P. Kharel, R. Naik, G. Lawes, *Philos. Mag. Lett.* **2007**, *87*(3–4), 223.

[25] . Kurnosov, V. Gnezdilov, P. Lemmens, Y. Pashkevich, A. K. Bera, A. T. M. N. Islam, B. Lake, *Low Temp. Phys.* **2017**, *43*(12), 1405.

[26] E. E. Sauerbrei, R. Faggiani, C. Calvo, *Acta Crystallogr. B* **1973**, *29*, 2304.

[27] A. P. Roy, S. K. Deb, M. A. Rekha, A. K. Sinha, *Indian J. Pure Ap. Phy.* **1992**, *30*(12), 724.

[28] G. Balakrishnan, O. A. Petrenko, M. R. Lees, D. M. Paul, *J. Phys. Condens. Matter* **2004**, *16*(29), L347.

[29] S. Baroni, P. Giannozzi, A. Testa, *Phys. Rev. Lett.* **1987**, *58*(18), 1861.

[30] G. Kresse, D. Joubert, *Phys. Rev. B* **1999**, *59*(3), 1758.

[31] A. Dal Corso, *Phys. Rev. B* **2010**, *82*(7), 075116.

[32] P. Hohenberg, W. Kohn, *Phys. Rev.* **1964**, *136*(3B), B864.

[33] W. Kohn, L. J. Sham, *Phys. Rev.* **1965**, *140*(4A), A1133.

[34] G. Kresse, J. Furthmüller, *Comput. Mater. Sci.* **1996**, *6*(1), 15.

[35] J. P. Perdew, K. Burke, M. Ernzerhof, *Phys. Rev. Lett.* **1996**, *77*(18), 3865.

[36] S. L. Dudarev, G. A. Botton, S. Y. Savrasov, C. J. Humphreys, A. P. Sutton, *Phys. Rev. B* **1998**, *57*(3), 1505.

[37] https://materialsproject.org/materials/mp-542151

[38] D. L. Rousseau, R. P. Bauman, S. P. S. Porto, *J. Raman Spectrosc.* **1981**, *10*(1), 253.

[39] R. Loudon, *Adv. Phys.* **1964**, *13*(52), 423.

SUPPORTING INFORMATION

Additional supporting information may be found online in the Supporting Information section at the end of the article.

How to cite this article: Kesari S, Rao R, Gupta MK, Mittal R, Balakrishnan G. Symmetries of modes in $Ni_3V_2O_8$: Polarized Raman spectroscopy and ab initio phonon calculations. *J Raman Spectrosc*. 2019;50:587–594. https://doi.org/10.1002/jrs.5539